

Stabilization mechanism of tetragonal structure in hydrothermal synthesized BaTiO₃ nanocrystal

Kenta Hongo,^{*,†,@} Sinji Kurata,[‡] Apichai Jomphoak,[¶] Miki Inada,[§] Katsuro Hayashi,[‡] and Ryo Maezono^{||,#}

[†]*Research Center for Advanced Computing Infrastructure, JAIST, Asahidai 1-1, Nomi, Ishikawa 923-1292, Japan*

[‡]*Department of Applied Chemistry, Faculty of Engineering, Kyushu University, Fukuoka 819-0395, Japan*

[¶]*National Electronics and Computer Technology Center (NECTEC), 112 Phahon Yothin, Klong Luang, Pathumthani 12120, Thailand*

[§]*Center of Advanced Instrumental Analysis, Kyushu University*

^{||}*School of Information Science, JAIST, Asahidai 1-1, Nomi, Ishikawa 923-1292, Japan*

[⊥]*National Institute for Materials Science (NIMS), 1-2-1 Sengen, Tsukuba, Ibaraki 305-0047, Japan*

[#]*Computational Engineering Applications Unit, RIKEN, 2-1 Hirosawa, Wako, Saitama 351-0198, Japan*

[@]*PRESTO, JST, 4-1-8 Honcho, Kawaguchi, Saitama 332-0012, Japan*

E-mail: kenta_hongo@mac.com

Abstract

Higher OH concentration is identified in tetragonal barium titanate (BaTiO₃) nanorods synthesized by a hydrothermal method with 10 vol% ethylene glycol solvent [Inada, M. *et al. Ceram. Int.* **2015**, *41*, 5581-5587]. This is apparently inconsistent with the known fact that higher OH concentration in the conventional hydrothermal synthesis makes pseudo-cubic BaTiO₃ nanocrystals more stable than the tetragonal one. To understand where and how the introduced OH anions are located and behave in the nanocrystals, we applied *ab initio* analysis to several possible microscopic geometries of OH locations, confirming the relative stability of the tetragonal distortion over the pseudo-cubic one due to the preference of trans-type configurations of OH anions. We also performed FTIR and XRD analysis, all being in consistent with the microscopic picture established by the *ab initio* geometrical opti-

mizations.

Introduction

The discovery of a classical ferroelectric barium titanate (BaTiO₃) dates back to the 1940s.¹⁻⁵ It has a tetragonal structure with a space group symmetry of *P4mm* at room temperature. Much attention has been paid to this material because of a variety of technical applications ranging from condensers to positive temperature coefficient (PTC) thermistors.⁶⁻⁹ For example, due to its high dielectric constant, BaTiO₃ is used as a dielectric layer of multilayer ceramic capacitors.^{8,9}

Hydrothermal synthesis¹⁰ is one of the widely used methods to obtain fine particles of BaTiO₃.¹¹ This method enables us to obtain highly pure fine powder with small particle size distribution and fairly stoichiometric composition.¹² In the conventional method, however, it

is known that there remains difficulty in controlling the crystal orientation (c -axis in the tetragonal structure) due to the particle size effect¹³ and the presence of OH groups in the shell region (surface and outer layer of crystal),^{13,14} yielding pseudo-cubic nanocrystals¹⁵ rather than the tetragonal ones. Extra thermal annealing at around 1,300 °C is known to be required to recover the tetragonal structure.¹⁶

Recently, Inada *et al.* have reported that a new hydrothermal scheme using 10 vol% ethylene glycol (EG)¹¹ directly produces tetragonal nanocrystals ($c/a = 1.013$) without any extra procedures. In the present work, we performed the thermal gravimetric analysis applied to the samples and then identified higher OH concentration inside 10 vol%-EG sample than 0 vol%-EG one. Doubt immediately rises over our finding because in the conventional hydrothermal synthesis, the OH inside BaTiO₃ nanocrystals has been widely regarded as having a role in stabilizing pseudo-cubic structure.¹³ We therefore performed an *ab initio* lattice relaxation analysis to investigate how the OH substitution stabilize tetragonal compared with pseudo-cubic.

We have found that the geometrical transition between *cis*- and *trans*- coordinations of substituted OH groups depends on their concentrations. The transition modifies Coulombic interactions of the OH substitutions with neighboring Ti cations as well as those with Ba vacancies introduced to compensate the charge neutrality. The relaxations due to the above modification can explain the trend of simultaneous contractions along a - and b -axes as well as elongations along c -axis when tetragonal structure is stabilized.

Experimental section

Synthesis

BaTiO₃ nanocrystals were obtained by a hydrothermal synthesis using Ba-Ti hydroxide precipitation as a precursor.¹¹ In the following, we provide minimum descriptions about our synthesis required for understanding further characterizations and theoretical analysis.

Detailed information is given in our preceding paper:¹¹ The concentration of Ba and Ti in the starting solution was adjusted to be 0.3 M (mol/L) and 0.2 M, respectively. First, 1 M BaCl₂ (15 mL) and 2 M TiCl₄ (5 mL) solutions were mixed at room temperature, followed by adding 10 M NaOH aqueous solution (10 mL) so as to precipitate Ba-Ti hydroxide. In order to obtain 50 mL of starting slurry, 20 mL of deionized (DI) water or 5 mL (10 vol%) of EG and 15 mL of DI water were added to the mixture. The starting slurry was placed into a 100 mL of Teflon-lined stainless steel autoclave and heated in an oven at 200 °C for 24 h, followed by cooling down in ice water. The products were separated, washed by decantation process repeatedly, and then dried at 60 °C overnight. Hereafter, the samples synthesized by the hydrothermal method with and without EG are denoted as EG-10 and EG-0, respectively. Actually, the nucleation and crystal growth of BaTiO₃ occurred via dissolution-reprecipitation. In our previous study,¹¹ we reported that the nucleation was suppressed by the addition of EG. The formation mechanism is also described in the literature.¹¹

Characterization

The powder X-ray diffraction (XRD) patterns were collected by X-ray diffractometer (Bruker AXS) with Cu K α radiation (40 kV, 40 mA) at room temperature. The lattice parameters were refined by a whole powder pattern decomposition (WPPD) method assuming a $P4mm$ structural model. The thermal behavior of the products was evaluated by thermogravimetric analysis (TGA). The OH groups were characterized by Fourier transform infrared (FTIR) spectroscopy.

Modeling and *Ab initio* calculations

The present study aims to investigate the stabilization mechanism of the tetragonal structure depending on the OH concentrations. To evaluate relative stability of Ba_{1-(1/2) x} TiO_{3- x} (OH) _{x} compounds with different amounts of substitutions x , we performed *ab initio* DFT

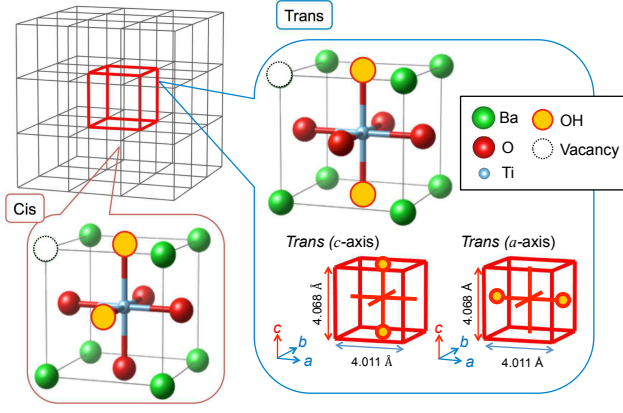


Figure 1: Modelling of 7% OH substitution with *cis*- and *trans*-coordinations by the $3 \times 3 \times 3$ supercell. For the latter, we considered the substitutions along *a*- and *c*-axis. Lattice constants shown in the figure are fixed at the experimental values obtained by X-ray diffractions (XRD).

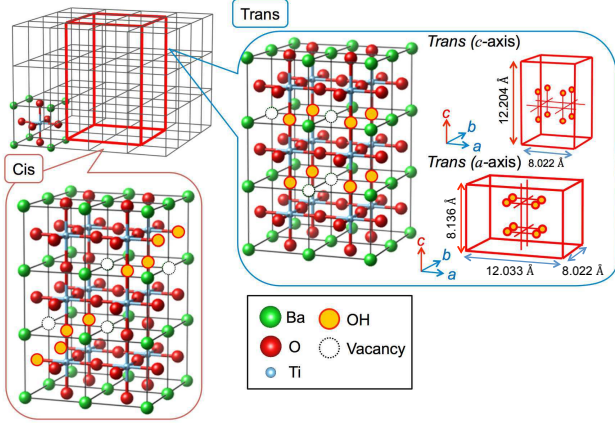


Figure 2: Modelling of 17% OH substitution with *cis*- and *trans*-coordinations by the $4 \times 4 \times 3$ supercell. For the latter, we considered the substitutions along *a*- and *c*-axis. Lattice constants shown in the figure are fixed at the experimental values obtained by X-ray diffractions (XRD).

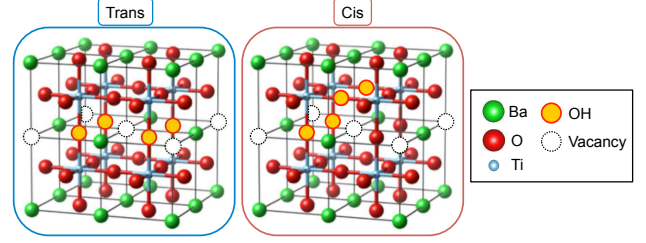


Figure 3: Modelling of 50% OH substitution with *cis*- and *trans*-coordinations by the $2 \times 2 \times 2$ supercell. For the latter, we considered the substitutions along *c*-axis.

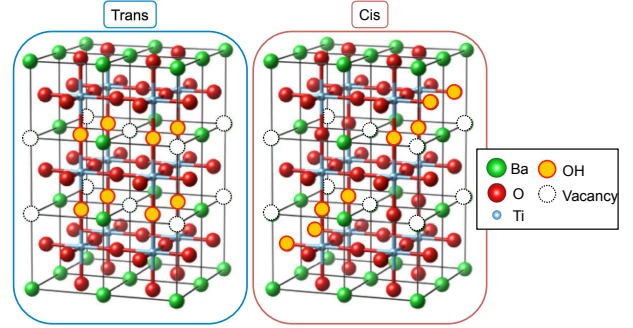


Figure 4: Modelling of 67% OH substitution with *cis*- and *trans*-coordinations by the $2 \times 2 \times 3$ supercell. For the latter, we considered the substitutions along *c*-axis.

simulations with the GGA/PBE¹⁷ exchange-correlation functional that has been well tested for both cubic and tetragonal phases of BaTiO₃.¹⁸ The amount of OH in synthesized BaTiO₃ was estimated from TGA. The experimental results strongly indicated only upto two substitutions, namely, *cis*- and *trans*- coordinations, as the possibilities we consider hereafter. The *c/a* value, calculated from XRD, of as-synthesized BaTiO₃ with EG was bigger than that of pure tetragonal BaTiO₃. And also, as-synthesized BaTiO₃ included a larger amount of OH than pure tetragonal. These experimental results indicate that the expand of *a* axis, that means the incorporation of OH along *a*-axis, is “not in accordance” with the experimental observation that the lattice constants of Ba_{1-(1/2)*x*}TiO_{3-*x*}(OH)_{*x*} elongate along *c*-axis compared with those of BaTiO₃. Thus, we compared only three possibilities of the substitutions, *i.e.*, OH located at the nearest neighbor [*cis*], or diagonal-wise along *a*-axis (*c*-axis) [*trans-a* (*trans-c*)] (see Fig. 1). On account of computability, we considered only four stoichiometric compounds of Ba_{1-(1/2)*x*}TiO_{3-*x*}(OH)_{*x*} (*x* = 0.07/0.17/0.50/0.67) within moderate sized simulation cells in which the numbers of O sites replaced by OH become integers. They were respectively modeled by 3×3×3, 4×4×3, 2×2×2, and 2×2×3 supercells, *i.e.*, by duplicating the original BaTiO₃ unit cell, as shown in Figures 1, 2, 3, and 4, respectively. To maintain the charge neutrality, Ba vacancies have to be introduced (all the possible patterns of locations are provided in Supporting Information). For the compensation of the neutrality, the reduction of a Ti⁴⁺ would be another possibility to realize the counter charge for the OH substitution. If that were the case, however, the powder color would get blueish, which is not observed in our synthesis. Moreover in general, Ba vacancies are easily introduced in the BaTiO₃ particles when synthesized by precipitation method because Ba ion is stable in alkaline condition of the reacting solution. These are the reason why we use the model of Ba vacancy and OH substitution. The model structures described above were generated by BIOVIA Materials Studio Visualizer,¹⁹ and

then the atomic positions within the simulation cells were further relaxed under the fixed lattice parameters (set as experimental value).

The geometry optimizations were carried out using the BFGS algorithm implemented in CASTEP²⁰ with thresholds for the energy convergence (1.0×10^{-3} eV/cell), the force convergence (0.05 eV/Å), the stress convergence (0.1 GPa), and the displacement convergence (0.002 Å). Monkhorst-Pack *k*-point meshes of 1×1×1, 1×1×1, 2×2×2, and 2×2×1 were adopted for the supercells with *x* = 0.07, 0.17, 0.15, and 0.67, respectively, each of which corresponds to *k*-point separation of 0.08 Å⁻¹. Ionic cores were described by the on-the-fly ultrasoft pseudo potentials implemented in CASTEP:²⁰ [He] for O, [Ne] for Ti, and [Kr]4*d*¹⁰ for Ba. Kohn-Sham orbitals were expanded in terms of planewaves with E_{cut} = 340 eV that is determined by the criterion that the total energy converges within 1.0×10^{-4} eV/cell.

Results and Discussion

Crystal structure of the BaTiO₃ nanocrystals and OH in those crystals.

Fig. 5 shows XRD patterns of the EG-10 and EG-0 samples. It was confirmed that the samples consist of a major phase of BaTiO₃ and a trace impurity of BaCO₃ as shown in Fig. 5 (a). The BaCO₃ impurity was formed by the reaction between Ba²⁺ and CO₃²⁻ dissolved from the atmosphere. The magnified view of the (200) and (002) reflections shown in Fig. 5 (b) reveals that these reflection peaks are clearly separated for the EG-10 sample while the one broad peak is observed for the EG-0 sample. This means that the EG-10 and EG-0 samples exhibit high and low tetragonality, respectively. It was also found that the diffraction angles of the EG-10 sample are lower than those of the EG-0 sample and bulk BaTiO₃ (dotted lines), indicating lattice expansion due to the incorporation of the OH groups in the crystals. Fig. 6 plots the content of OH groups determined by TGA along with the *c/a* ratio as a function

of heat-treatment temperature. The content of OH groups in the EG-10 sample is about three times as many as that in the EG-0 sample. The EG-10 sample has a higher c/a ratio than that of bulk BaTiO_3 , indicating the enhancement of tetragonality due to the incorporation of the OH groups. The OH content and the c/a ratio decrease with increasing heat-treatment temperature up to 800 °C, suggesting a significant correlation between the content of OH groups and the c/a ratio of the BaTiO_3 crystals.

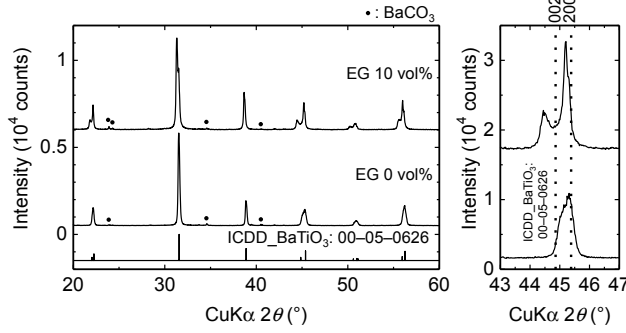


Figure 5: X-ray diffraction (XRD) patterns of BaTiO_3 synthesized with and without ethylene glycol (EG-10 and EG-0, respectively). (a) Whole area and (b) selected area that indicates reflections from (200) planes. Dotted lines show peak positions of (200) and (002) directions from ICDD: 00-005-0626.

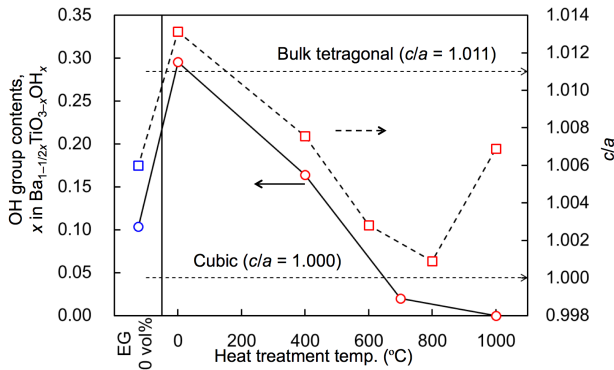


Figure 6: Changes in OH contents and c/a of BaTiO_3 synthesized with 10 vol% EG versus heat treatment temperature. Blue plots indicate the results without EG.

Characterization of the OH groups in the crystals by FTIR and DFT calculations

FTIR (Fourier transform infrared spectrometer) analysis was carried out in order to characterize the OH groups in the crystals. The result is shown in Fig. 7. We found a peak around at 3500 cm^{-1} , which can be deconvoluted with a slightly sharp peak around at 3480 cm^{-1} and a broad peak around at 3350 cm^{-1} , indicating that there are two kinds of OH groups in the crystals. The peak area intensity of the EG-10 sample is larger than that of the EG-0 sample; in particular, the area intensity of the peak around at 3480 cm^{-1} is much larger for the EG-10 sample than for the EG-0 sample. As explained later, our DFT gives two different relaxed positions of substituted OH, which can be identified to each of peaks, namely, 3480 cm^{-1} being attributed to OH- V_{Ba} defect complexes, and 3350 cm^{-1} to OH...O hydrogen bonds. The area intensity of a peak around at 3480 cm^{-1} decreases by heat treatment as shown in the inset of Fig. 7.

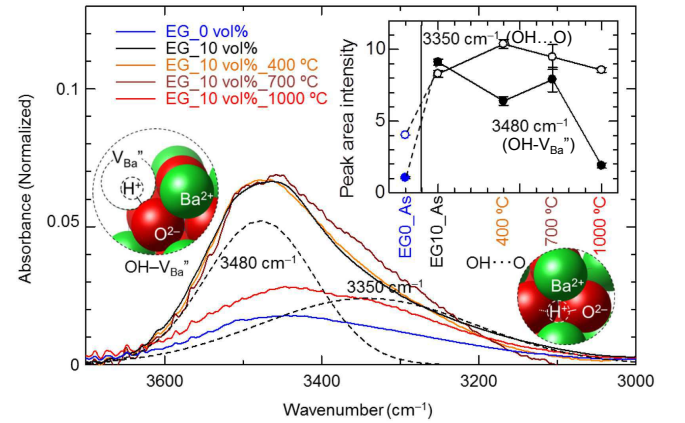


Figure 7: FTIR spectra of the OH groups in the BaTiO_3 nanocrystals synthesized with 10 vol% EG before and after heat treatment at 400-1000 °C. For comparison, the result without EG is also shown in blue line. The peak area intensities versus the heat treatment temperatures are inset.

Ab initio Analysis

Ab initio analysis was carried out to gain microscopic insights into how the substituted OH-sites play a role in stabilizing the tetragonal crystal structure. As explained in the previous section, we prepared four different supercells to model various substitution, x . We compared the energies of *cis*- and *trans*- coordinations of OH-substituents as a function of x as shown in Fig. 8. We see that the relative stability inverts as the substituent concentration x increases.

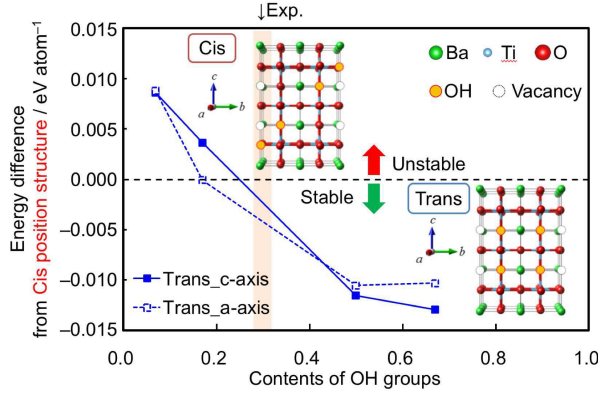


Figure 8: The total energies of the *trans*- coordinations along *a*- and *c*-axes with respect to that of the *cis*- coordinations. The region above the broken line indicates the *cis*- coordination is stable. The region below the broken line indicates the *trans*- coordination is stable.

The fact that the *trans*- coordination gets more stable for larger x can be roughly connected with the *physical pictures* of the distortion caused by the OH-substitution. Figures 9 and 10 show how the elongations of O-Ti-O bond lengths appear around the OH-sites with different concentrations, $x = 0.07$ and $x = 0.5$, respectively. While the distortion occurs locally around the OH-sites for the smaller x (Fig. 9), it spreads over the whole system uniformly for the larger x (Fig. 10). The latter has a large enough number of the OH-sites to get the distortions cooperatively accommodated within the system, which makes energy loss less than the former where the local distortion causes the energetically unstable state.

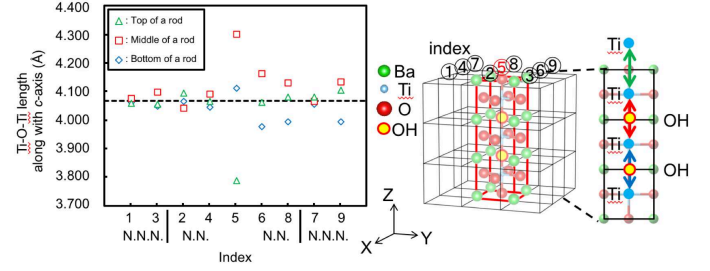


Figure 9: Spatial relaxations of the elongated bonding lengths along *c*-axis, evaluated at $x=0.07$ described by $3 \times 3 \times 3$ supercell. Right panel gives the convention of indexing for the 'rods', O-Ti^(top)-O-Ti^(center)-O-Ti^(bottom)-O, along *c*-axis. Upper and lower sides of Ti^(center) at 'rod#5' are substituted into OH (*trans*-coordination). Lengths of O-Ti^(top)-O, O-Ti^(center)-O, and O-Ti^(bottom)-O are plotted in the left panel, showing the local distortion at the substituted site is relaxed down over the nearest neighbors (N.N.) and the next nearest neighbors (N.N.N.).

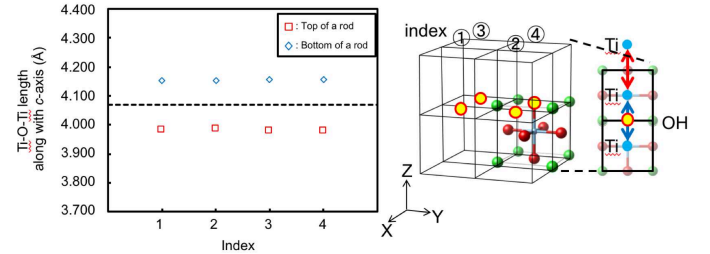


Figure 10: For the larger x (OH concentration), the distortions due to the OH substitutions (changes in the bonding lengths along *c*-axis) are cooperatively occurs over the crystal. Right panel gives the convention of indexing for the 'rods', O-Ti^(top)-OH-Ti^(bottom)-O, along *c*-axis. The bond lengths are evaluated at $x = 0.5$ described by $2 \times 2 \times 2$ supercell, plotted in the left panel over the rods #1~#4.

Fig. 11 shows the lattice relaxation around the substituted OH-site, evaluated by $3 \times 3 \times 3$ supercell with $x = 0.07$. From Figures 9 and 10, we could see two possible effects of causing distortions by the substituents, '(a) OH-site solely gets attracted by the vacancy V_{Ba} ' and '(b) the *trans* location of two OH along *c*-axis gets the OH-Ti-OH bond elongated along the axis'. The effect (a) could be explained by the fact that the vacancy would be charged negatively if the positive Ba^{2+} ion was not there, attracting a proton of a OH ion via electrostatic interactions. Comparing the relaxations of OH positions with and without V_{Ba} nearby (left and right panels of Fig. 11), we can see the formation of the hydrogen bonding between OH and nearest-neighbor O-site when without vacancy. This contrast would explain two different absorption peaks in FTIR (Fig. 7) at 3480 cm^{-1} and 3350 cm^{-1} . The latter peak would be identified to the lattice vibrations with weakened coupling due to the formation of the hydrogen bonding.

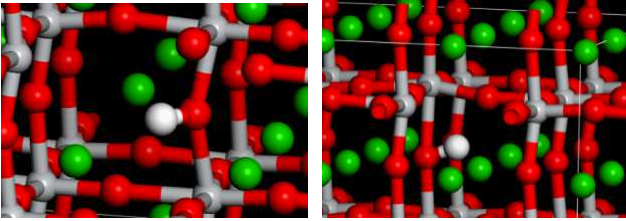


Figure 11: Local relaxations of atomic positions around the substituted OH, evaluated at $x = 0.07$ described by $3 \times 3 \times 3$ supercell. White (red) balls represent H (O) atoms. Two cases with and without a Ba vacancy are shown in left and right panels, respectively. In the former case, the OH is found to be attracted toward the vacancy due to its positively charged background. In the latter case instead, the OH is attracted toward the neighboring O to form hydrogen bondings.

The effect (b), the elongation of OH-Ti-OH bond, could be qualitatively understood as a consequence of the weakened electrostatic interaction with Ti caused by replacing O^{2-} with OH^- . The displacement of Ti is, however, found to be small being around $1.049 \sim 1.060$

in terms of the ratio of the longer Ti-O bond length to the shorter one (Fig. 10). The smaller displacement would be explained as follows: Since the larger displacement of Ti from its original center would yield the two larger dipole moments in the opposite direction, the resultant dipole-dipole interactions could give rise to an increase in the system energy. Thus, the possible displacement remains within the smaller amount so as to prevent the system from increasing the energy.

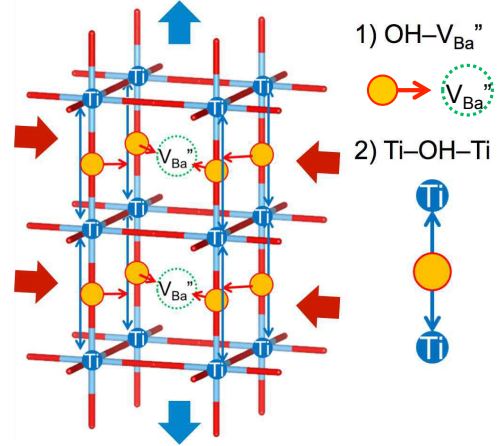


Figure 12: A schematic picture showing how the substituted OH stabilizes the tetragonal structure with higher concentration. They are attracted toward a Ba vacancy, which emerges to realize the charge neutrality, yielding contractions of *a* and *b* bond lengths. On top of that, the reduction in the negative stoichiometric charge ($O^{2-} \rightarrow OH^-$) brings about the elongation of bonding length along *c*-axis.

The above effects, '(a) attraction of OH by V_{Ba} ' and '(b) elongation of OH-Ti-OH bonds', would explain the trend in stability of the tetragonal structure relative to the pseudo-cubic one depending on the OH concentration, x . For the region where the *cis*-coordination is stabilized, *e.g.*, $x = 0.07$, the OH-sites get attracted toward the Ba-vacancies individually and uniformly, giving rise to the pseudo-cubic structure. For the larger x , *e.g.*, $x = 0.25$, where the *trans*-coordination is stabilized instead, the effect (a) promotes the contraction of *a*- and *b*-axis (see Fig. 12), while the effect (b) yields the elongation along *c*-axis, resulting

in the stabilization of the tetragonal structure. Thermal gravimetric analysis (TGA) applied to the present EG-synthesized samples estimates $x \sim 0.28$, dropping at the region where the tetragonal structure gets stabilized, being consistent with the experimental fact.

The above scenario is not contradicting to the fact that the conventional hydrothermal synthesis gives pseudo-cubic nanocrystals even with higher x as long as we regard it as the 'core-shell' structure¹³ where the doped OHs are not incorporated into the 'core' region but located only at the 'shell' (surface of the core) randomly. The present analysis using super-cells corresponds to the assumption that the doped OHs are located uniformly inside the entire crystal, being the case only for the EG-synthesized sample.

Conclusion

We investigated the role of substituted OH in stabilizing tetragonal anisotropy of the BaTiO₃ nanocrystal synthesized by a hydrothermal scheme using ethylene glycol (EG). Thermogravimetric analysis was carried out to identify the concentration of OH, revealing that the EG-synthesized sample has around three times larger amount of OH concentration compared to the sample synthesized by the conventional hydrothermal scheme. Since in the conventional scheme the introduced OH has been regarded as playing a role in stabilizing the pseudo-cubic isotropic structure, the present tetragonal anisotropic structure involving the large amount of OH concentration stimulated curiosity.

The apparent contradiction is finally attributed to how the introduced OH groups are distributed throughout a sample. Employing structural models with uniform OH distributions, our *ab initio* geometrical relaxation analysis concluded the stabilization of tetragonal anisotropy in the higher OH concentration range where the *trans*-coordinations of substitutions were preferred. In pseudo-cubic nanocrystals synthesized by the conventional scheme, in-

stead, the introduced OH can be thought of as being distributed only within the 'shell' region over the 'core' region, not uniformly, and hence the present analysis is beyond the scope of the core-shell interpretation.

The predicted stabilization was explained by several mechanisms such as, the cooperative accommodation of the lattice deformations, electrostatic interactions between Ba vacancies and OH, and the elongation along the *trans*-coordination of OHs due to less attraction between anion site and Ti caused by the reduction in negative charge from O²⁻ to OH⁻.

Author information

Competing financial interests: The authors declare no competing financial interests.

Supporting Information

All the possible patterns of Ba vacancies and OH anions in Ba_{1-(1/2)x}TiO_{3-x}(OH)_x ($x = 0.07/0.17/0.50/0.67$) are provided, which is mentioned in "Modeling and *Ab initio* calculations". This information is available free of charge via the Internet at <http://pubs.acs.org>.

Acknowledgement

This work was supported by the Grant-in-Aid for Scientific Research on Innovative Areas "Mixed Anion" project (JP16H06439, JP16H06440 and 17H05478) from MEXT. All the computation in this work has been performed using the facilities at Research Center for Advanced Computing Infrastructure in JAIST. The FTIR analysis was carried out using FTIR620 at the Center of Advanced Instrumental Analysis, Kyushu University. K. Hongo is also grateful for financial support from a KAKENHI grant (17K17762), PRESTO (JP-MJPR16NA) and the Materials research by Information Integration Initiative (MI²I) project of the Support Program for Starting Up Innovation Hub from Japan Science and Technology Agency (JST). R.M. is also grateful for financial

supports from MEXT-KAKENHI (16KK0097), from FLAGSHIP2020 (project nos. hp170269 and hp180175 at K-computer), from Toyota Motor Corporation, from I-O DATA Foundation, and from the Air Force Office of Scientific Research (AFOSR-AOARD/FA2386-17-1-4049). K.Hayashi is supported by Elements Strategy Initiative to Form Core Research Center, MEXT, Japan.

References

- (1) Wainer, E.; Salomon, A. Titanium Alloy Manufacturing Co., Electrical Report 8, 1942.
- (2) Wainer, E.; Salomon, A. Titanium Alloy Manufacturing Co., Electrical Report 9, 1943.
- (3) Ogawa, T. *Busseiron Kenkyu (in Japanese)* **1947**, 6, 1–27.
- (4) Wul, B.; Goldman, J. Dielectric Constants of Titanates of Metals of the Second Group. *Dokl. Mad. Nauk. SSSR* **1945**, 46, 154.
- (5) Cross, L. E.; Newnham, R. E. *Ceramics and Civilization, Volume III*; pp 289–305.
- (6) Saburi, O. Properties of Semiconductive Barium Titanates. *Journal of the Physical Society of Japan* **1959**, 14, 1159–1174.
- (7) SABURI, O. Semiconducting Bodies in the Family of Barium Titanates. *Journal of the American Ceramic Society* **1961**, 44, 54–63.
- (8) Burn, I.; Maher, G. H. High resistivity BaTiO₃ ceramics sintered in CO-CO₂ atmospheres. *Journal of Materials Science* **1975**, 10, 633–640.
- (9) Sakabe, Y.; Minai, K.; Wakino, K. High-Dielectric Constant Ceramics for Base Metal Monolithic Capacitors. *Japanese Journal of Applied Physics* **1981**, 20, 147.
- (10) Pinceloup, P.; Courtois, C.; Leriche, A.; Thierry, B. Hydrothermal Synthesis of Nanometer-Sized Barium Titanate Powders: Control of Barium/Titanium Ratio, Sintering, and Dielectric Properties. *Journal of the American Ceramic Society* **1999**, 82, 3049–3056.
- (11) Inada, M.; Enomoto, N.; Hayashi, K.; Hojo, J.; Komarneni, S. Facile synthesis of nanorods of tetragonal barium titanate using ethylene glycol. *Ceramics International* **2015**, 41, 5581 – 5587.
- (12) Hayashi, H.; Hakuta, Y. Hydrothermal Synthesis of Metal Oxide Nanoparticles in Supercritical Water. *Materials* **2010**, 3, 3794–3817.
- (13) Hoshina, T.; Wada, S.; Kuroiwa, Y.; Tsurumi, T. Composite structure and size effect of barium titanate nanoparticles. *Applied Physics Letters* **2008**, 93, 192914.
- (14) Petkov, V.; Gateshki, M.; Niederberger, M.; Ren, Y. Atomic-Scale Structure of Nanocrystalline Ba_xSr_{1-x}TiO₃ ($x = 1, 0.5, 0$) by X-ray Diffraction and the Atomic Pair Distribution Function Technique. *Chemistry of Materials* **2006**, 18, 814–821.
- (15) Yan, T.; Shen, Z.-G.; Zhang, W.-W.; Chen, J.-F. Size dependence on the ferroelectric transition of nanosized Ba-TiO₃ particles. *Materials Chemistry and Physics* **2006**, 98, 450 – 455.
- (16) Sasirekha, N.; Rajesh, B. a. Hydrothermal Synthesis of Barium Titanate: Effect of Titania Precursor and Calcination Temperature on Phase Transition. *Industrial & Engineering Chemistry Research* **2008**, 47, 1868–1875.
- (17) Perdew, J. P.; Burke, K.; Ernzerhof, M. Generalized Gradient Approximation Made Simple. *Phys. Rev. Lett.* **1996**, 77, 3865–3868.

- (18) Bilc, D. I.; Orlando, R.; Shaltaf, R.; Rignanese, G.-M.; Íñiguez, J.; Ghosez, P. Hybrid exchange-correlation functional for accurate prediction of the electronic and structural properties of ferroelectric oxides. *Phys. Rev. B* **2008**, *77*, 165107.
- (19) BIOVIA Materials Studio Visualizer. <http://accelrys.com/products/collaborative-science/biovia-materials-studio/>, Accessed: 2017-12-18.
- (20) Clark, S. J.; Segall, M. D.; Pickard, C. J.; Hasnip, P. J.; Probert, M. I. J.; Refson, K.; Payne, M. C. First principles methods using CASTEP. *Zeitschrift für Kristallographie - Crystalline Materials* **2005**, *220*, 567 – 570.